

Noise mitigation methods for ion detectors operating with a direct view of high temperature plasmas

P. J. Fimognari, T. P. Crowley, D. R. Demers, and T. D. Kile

Citation: [Review of Scientific Instruments](#) **89**, 101108 (2018); doi: 10.1063/1.5039348

View online: <https://doi.org/10.1063/1.5039348>

View Table of Contents: <http://aip.scitation.org/toc/rsi/89/10>

Published by the [American Institute of Physics](#)

Articles you may be interested in

[Thin foil proton recoil spectrometer performance study for application in DT plasma measurements](#)

[Review of Scientific Instruments](#) **89**, 101107 (2018); 10.1063/1.5038924

[High detection efficiency scintillating fiber detector for time-resolved measurement of triton burnup 14 MeV neutron in deuterium plasma experiment](#)

[Review of Scientific Instruments](#) **89**, 101101 (2018); 10.1063/1.5032118

[The neutron camera upgrade for MAST Upgrade](#)

[Review of Scientific Instruments](#) **89**, 101110 (2018); 10.1063/1.5038948

[Scintillating fiber detectors for time evolution measurement of the triton burnup on the Large Helical Device](#)

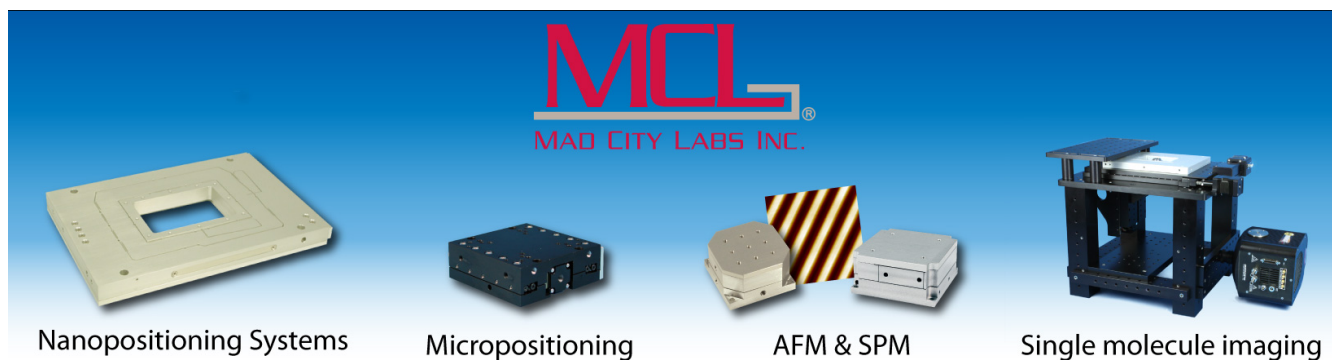
[Review of Scientific Instruments](#) **89**, 101105 (2018); 10.1063/1.5035290

[First measurements of a scintillator based fast-ion loss detector near the ASDEX Upgrade divertor](#)

[Review of Scientific Instruments](#) **89**, 101106 (2018); 10.1063/1.5038968

[Effect of neutron and \$\gamma\$ -ray on charge-coupled device for vacuum/extreme ultraviolet spectroscopy in deuterium discharges of large helical device](#)

[Review of Scientific Instruments](#) **89**, 101109 (2018); 10.1063/1.5037233



MCL
MAD CITY LABS INC.

Nanopositioning Systems Micropositioning AFM & SPM Single molecule imaging

Noise mitigation methods for ion detectors operating with a direct view of high temperature plasmas

P. J. Fimognari,^{a)} T. P. Crowley, D. R. Demers, and T. D. Kile
Xantho Technologies, LLC, Madison, Wisconsin 53705, USA

(Presented 16 April 2018; received 7 May 2018; accepted 12 July 2018;
 published online 27 August 2018)

We have developed an ion current measurement instrument with a direct view of a plasma that reduces the particle and radiation-induced noise current it detects by over three orders of magnitude, from tens of microamps to tens of nanoamps. This is accomplished using electric fields, magnetic fields, and physical shielding that limit the flux of particles and radiation into the instrument and suppress the secondary electrons produced within it by particle and radiation impact. Operation of this detector in various configurations, without an ion beam, has allowed identification of the sources of noise current. In our experimental setup, the largest noise contributors were found to be plasma ions and photoelectric emission due to UV radiation. *Published by AIP Publishing.* <https://doi.org/10.1063/1.5039348>

I. INTRODUCTION

We are developing an instrument^{1,2} to measure the current of high energy, high mass (e.g., 45 keV K⁺⁺) ions created through the interaction of a diagnostic beam with a magnetically confined high temperature plasma. It measures the position and entrance angle^{3,4} (used to determine a component of velocity) of the ions. Data obtained with the instrument will be used to infer information about the plasma magnetic field, density, and temperature. It is intended to operate in plasma facing ports, beamlines, or other locations with a direct view of a plasma. This exposes it to stray particles and radiation, which can cause significant noise signals. During initial development, the instrument has been tested in a region with a very weak background magnetic field. In this paper, we present an overview of the instrument and discuss the methods used to mitigate noise signals. They enable our instrument to resolve desired ion current and may be of value for other ion detection applications.

II. THE CHALLENGE

To obtain meaningful data, noise current levels should be less than the (desired measurement) signal current (which for our present application is on the order of 10-100 nA). Without the noise reduction features of our instrument, the undesired noise current has typically been 10-100 μ A, with excursions to milliamp levels.

The instrument is sensitive to charged particle current and cannot distinguish between an electron leaving and an ion impacting its detector elements. Currents measured with the instrument originate from several sources, illustrated in Fig. 1, including the diagnostic beam, the plasma, nearby surfaces, and the detector elements. Beam ions that impact detector elements and the secondary electrons they create

are the desired signal; we consider all other currents to be undesired noise. This noise consists of charged particles impacting or leaving detector elements and includes positive currents (due to the plasma ions, ions created in the instrument through photoionization, and secondary electrons leaving detector elements) and negative currents (due to secondary electrons that are created on nearby surfaces and travel to detector elements). Secondary electrons are created when stray ions, beam ions, and direct or reflected UV radiation impact metallic surfaces within or surrounding the instrument. A significant challenge in development of our instrument has been reducing the undesired noise to enable measurements.

Table I lists the noise sources, categorized by the charged particle that is responsible, and their associated energy ranges. It identifies the methods we have used to mitigate them (if applicable), namely, electric and magnetic fields. It also lists the location within this paper (or elsewhere) where more detailed discussion of the noise source is located.

The noise mitigation features that we have developed for this instrument are enabling measurement of ions in the presence of stray particles and radiation near a fusion plasma boundary. Other fusion diagnostics that measure particle properties, such as fast ion loss detectors (FILDs) and electrostatic analyzers,⁶ can experience similar undesired signal challenges and may benefit from the noise mitigation features we have developed.

III. OUR SOLUTION

A. The prototype instrument

We have prototyped a series of instruments having similar geometry. Figure 2 shows (a) an exploded view and (b) a side cross section of the most recent version of the instrument, which measures 156 \times 75 \times 64 mm and has all the noise mitigation features discussed in this paper. Components are color-coded by their electromagnetic character: elements held at ground potential are gray (*a*, *d*), insulators

Note: Paper published as part of the Proceedings of the 22nd Topical Conference on High-Temperature Plasma Diagnostics, San Diego, California, April 2018.

^{a)}Author to whom correspondence should be addressed: PJFimognari@XanthoTechnologies.com.

PREDOMINANT SOURCES OF CURRENT

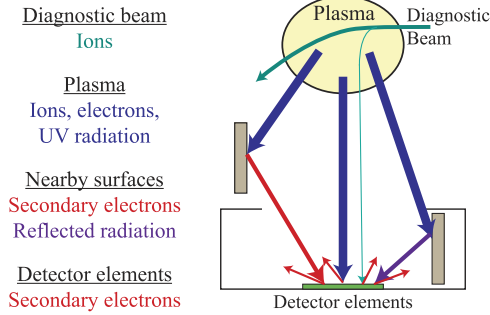


FIG. 1. Illustration of sources that may result in measured current signals. For an instrument with a direct view of a plasma, currents other than the desired diagnostic beam signal can dominate measurements.

are blue (*i*), detector elements (which are connected to transimpedance amplifiers for current measurement) are green (*b*, *c*), electrodes are red (*f*, *g*), and permanent magnets are cyan (*e*, *h*).

Our prototype instrument measures beam ions that pass through (*a*) an aperture-set and impinge upon two parallel planes of detector elements, made of stainless steel. These are (*b*) the detection grating and (*c*) the split-plates. The method used to convert the currents measured by these detector elements into physical quantities is described in Ref. 1. The remaining labeled components (*d-i*) all are designed to enable our instrument to operate with a direct view of a plasma by reducing undesired noise. The aperture-set, the split-plate support plate, and a magnet flux-keeper form a box that divides the instrument into two regions, external and internal. The aperture-set contains the only significant openings between the two regions. The external region consists of the surrounding (*d*) external shielding; the external aperture, flanked by a pair of (*e*) external permanent magnets; and (*f*) the electrostatic grating. In the internal region are (*g*) two electrostatic gratings, (*h*) internal permanent magnets above and below the (detection grating and split-plate) detector elements, and (*i*) insulating shields surrounding the metal support arms of the detection grating. These noise reduction

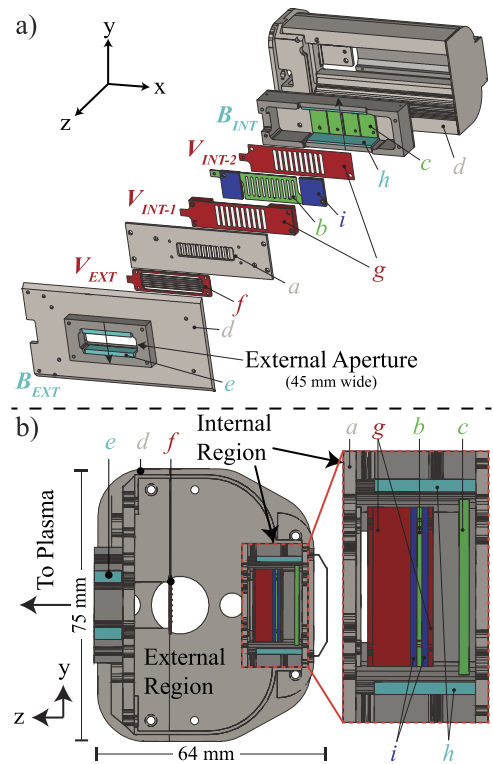


FIG. 2. (a) An exploded view and (b) a side cross section of the prototype instrument showing the noise mitigation components and permanent magnet field directions. All gray colored parts are held at ground potential, blue colored elements are insulating, and green components are connected to transimpedance amplifiers. Two pairs of magnets (colored cyan) are sources of local magnetic fields (B_{EXT} , B_{INT}), and three electrodes colored red are biased (V_{EXT} , V_{INT-1} , and V_{INT-2}).

features fall into two categories: particle and radiation mitigation and secondary electron suppression, which are described in Sec. III B.

B. Noise reduction methods

1. Particle and radiation mitigation

This method of noise reduction focuses on features that reduce the quantity of particles and radiation that enter the

TABLE I. Noise sources, mitigation methods, and reference or section of this article containing additional discussion.

Charged particle current	Noise source	Energy range (eV)	Mitigation method	Discussed in section
Ions	Plasma	0-1	Port-hole permanent magnets ⁵	Reference 5
		1-500	External permanent magnets and electrostatic grid	Section III B 1
		>500	None	N/A
Electrons	Photoionization and acceleration within instrument	0-500	Bias voltage optimization	Section IV A
		Radiation or particle impact on detector elements	Internal permanent magnets and electrostatic grids, bias voltage optimization	Section III B 2

instrument. The first of these is a surrounding, electrically grounded, external shield (d in Fig. 2) made of stainless steel. This shield has a few gaps, the largest of which is the 45×12 mm external aperture through which particles, radiation, and beam ions can pass.

The second method used to reduce noise is a magnetic field. To reduce an undesired particle flux through the external aperture, we use a pair of rectangular nickel-plated NdFeB permanent magnets (e in Fig. 2, N30 grade, field oriented in the $-y$ direction) in a 1018 mild steel flux-keeper, which concentrates the magnetic field to the external aperture. The magnetic field along a line midway between the magnets ($y = 0$) at the center of the external aperture in the z direction was measured to be 2.3 kG at the center ($x = 0$) and 1.7 kG at $x = \pm 15$ mm.

The trajectories of stray low energy ions and essentially all electrons are greatly altered by this magnetic field, while (high energy, large mass) beam ions are only modestly perturbed. Rough calculations indicate that electrons with energy less than 150 keV (which should account for all electrons in the vicinity of the instrument) and deuterium ions with energy less than 40 eV are effectively stopped, but the velocity of a 45 keV K^{++} ion is changed by less than 1° .

The field from the magnets is not able to stop all incoming ions; we use an electrostatic grating (f in Fig. 2) directly behind the external aperture to stop stray ions of higher energy. The grating consists of a stainless steel frame with wires spot-welded into machined grooves to provide a uniform electric field. It is biased up to $V_{EXT} = 500$ V. This grating also attracts photoelectrons produced by UV striking walls of the instrument in the external region, which may further reduce the particle flux onto the detector elements.

2. Secondary electron suppression

Even with particle and radiation mitigation at the entrance to the instrument, the noise current measured by our prototype was more than two orders of magnitude greater than the desired level. Having eliminated most particle flux into the instrument with the features discussed in Sec. III B 1, the remaining noise is largely secondary electrons induced by UV radiation. Other possible sources of noise, such as photoionized gas particles produced within the instrument, are expected to be small.

UV photons that make their way into the instrument can liberate secondary electrons from either detector elements or other parts of the instrument and cause noise currents. When UV impacts detector elements, secondary electrons liberated from them will be measured as a positive current. Electrons photoemitted from other surfaces within the instrument that subsequently impact detector elements will be measured as a negative current.

Our methods to suppress secondary electrons within the internal region of the instrument are, again, applications of magnetic and electric fields. A pair of nickel-plated NdFeB permanent magnets (h in Fig. 2, N45 grade, field oriented in the $+y$ direction) are installed in the internal region of the instrument above and below the detector elements, insulators, and internal electrodes. As with the external magnets,

a flux-keeper is used to concentrate the field. The magnetic field at the z location of the detection grating varies from 700 G to 880 G on a line midway between the magnets ($y = 0$), oriented in the direction opposite to that of the external magnets to have the opposite effect on the beam ions (i.e., beam ions deflected left by the external magnets are deflected right by the internal ones). Most secondary electrons produced through beam and photon impact are of low energy (< 20 eV). A 20 eV electron emitted in a 700 G field will have a Larmor radius of 0.2 mm. The distances between components in the instrument are ≥ 0.8 mm; thus, the Larmor orbit of most electrons will return them to their emitting surface. Assuming that the magnetic field is nearly parallel to the detector element surfaces, approximately 75% of photoelectrons and 95% of particle-produced secondary electrons (including those produced by beam ions) are expected to impact their emitting surface in less than one Larmor orbit. The rates of the two populations differ due to their initial velocity distributions (photoelectrons are expected to be mostly parallel to the electric field of the incoming photon while particle-liberated secondary electrons have a more uniform distribution).

An electric field is applied within the internal region by biasing the internal electrostatic gratings (g in Fig. 2). In experiments without the magnetic field described in the previous paragraph, the electric field pushes secondary electrons back to their emitting surfaces when the electrodes are biased at a negative potential. When applied along with the magnetic field, an $E \times B$ drift is introduced to the secondary electron motion. Electrostatic biasing has been used successfully on other devices to control secondary electron emission as well.⁷⁻⁹

The detection grating has metal support arms that extend beyond the magnetic field, and secondary electron suppression is not as effective in that region. This resulted in larger noise levels on the detection grating than on the split-plates. Insulating shields (i in Fig. 2) were installed to cover these support arms and block the path of unsuppressed electrons. This reduced the noise on the grating to a level similar to the split-plates.

IV. EXPERIMENT

A. Environment and setup

The Madison Symmetric Torus (MST) Reversed Field Pinch at the University of Wisconsin, Madison,¹⁰ has served as the test-bed for our instrument development. MST exhibits large neutral (100-200 kW), convective particle (1.3-1.4 MW), and radiative (200 kW)¹¹ fluxes. The measurements discussed in this paper were acquired during ohmically heated improved confinement plasmas with $I_p \approx 380$ kA and $n_e \approx 6 \times 10^{12}$ cm⁻³. An ion beam was not used.

Our instrument is located in the (secondary) detection beamline (stainless steel vacuum chambers with a diameter of ~ 25 cm) of the heavy ion beam probe (HIBP) diagnostic.¹² It is ~ 50 cm from the MST plasma and views the plasma through a 4.5'' diameter port. A permanent magnet plasma suppression structure⁵ at the MST porthole provides a massive reduction of the flux of plasma particles (particularly electrons) to our

prototype instrument. The structure also reduces the field-of-view to the plasma from a 114 mm diameter circle to approximately 80×110 mm.

In addition to the hardware features of the instrument described in Sec. III B, an operational technique in which we optimize internal electrostatic grating (g) voltages is used to achieve a balance between the noise currents arriving at and leaving the detector elements. Biasing the gratings at a zero or positive voltage results in positive noise currents on the detector elements (suggesting a net outflow of electrons), while operating the gratings at a large negative voltage results in negative noise current on the detector elements (suggesting an influx of electrons). Operating the gratings with a negative bias between -10 V and -40 V results in an average noise current close to 0 and a reduced noise current variability. This is consistent with findings from other ion detectors.⁹

B. Experimental results

A series of experiments to investigate noise and mitigation methods were performed using various prototype configurations without the diagnostic beam. Eight of these, which we refer to as A-H, were similar to the prototype shown in Fig. 2 (which is config. H). These configurations differed in which components (labeled d , e , h , and i in Fig. 2) were installed and in the potential at which the bias gratings (labeled f and g in Fig. 2) were held; key differences are captured in Table II. For example, config. A did not have any permanent magnets (e , h) or shielding (d , i) installed.

For this work, we are primarily concerned with minimizing the quantity of noise measured by the instrument and not fine-tuning the distribution among its elements. Hence the quantity of greatest interest is the total current measured by the detector elements (i.e., the sum of the detection grating

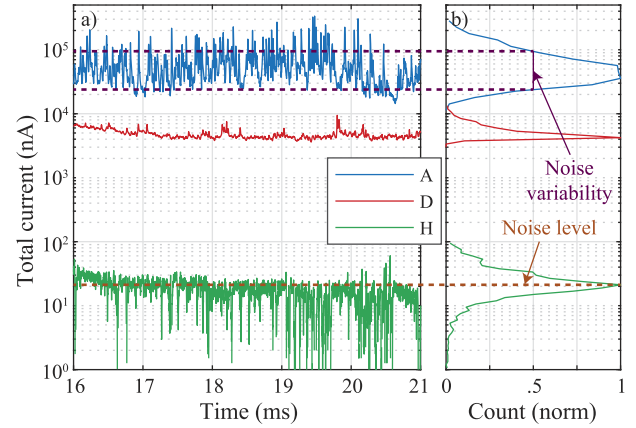


FIG. 3. Total current measured with the instrument in configs. A, D, and H as (a) time series and (b) histogram (normalized to the peak of the distribution) plots. Defined from the (b) histograms are the noise level (which is the most common value of the current, depicted for config. H) and the noise variability (the FWHM of the histogram, depicted for config. A). Dashed lines indicating the noise level and upper and lower limits of the FWHM are mapped back to the time-series plot.

and split-plates currents), which is described in the following paragraphs.

Figure 3 shows (a) time series and (b) histogram plots (normalized to the peak of the distributions) of the total current measured with the instrument in three configurations (A, D, and H). The total current shows a slow time-varying behavior over the improved confinement period and a series of noise spikes. The histogram is used to quantify the character of the noise using two parameters; we define the noise level as the peak of the current distribution and the noise variability as the full width of the histogram at half of the peak value.

TABLE II. Comparison of the noise levels and variability for the instrument configured with and without (a) particle and radiation mitigation features and (b) secondary electron suppression features installed. Components f and g were installed in all configurations, and bias voltages are listed. Use of shielding, permanent magnets, and biased electrodes, when compared with config. A, results in a reduction in the magnitude of noise current of more than one order of magnitude for config. D and three orders of magnitude for config. H.

(a) Particle and radiation mitigation components installed						
Prototype components						
Config.	d External shielding	e B_{EXT}	f V_{EXT} (V)	Noise level (μA)	Noise var. (μA)	
A	No	No	0	47	64	
B	No	No	100	13	24	
C	Yes	Yes	0	4.3	3.1	
D	Yes	Yes	500	4.3	1.5	
(b) Secondary electron suppression components installed						
Prototype components						
Config.	g V_{INT-1} (V)	h V_{INT-2} (V)	i B_{INT}	i Insulating shields	Noise level (nA)	Noise var. (nA)
D	0	0	No	No	4300	1500
E	-10	-10	No	No	-52	140
F	0	0	Yes	No	360	110
G	-10	-15	Yes	No	0	80
H	-40	-20	Yes	Yes	20	21

A subset of our experimental results for configs. A-H is captured in Table II. In this table, an ensemble of measurements of noise levels and variability from all improved confinement periods matching the conditions noted in a given row are shown in the rightmost two columns.

Table II(a) shows the result of tests comparing particle and radiation mitigation features in the external region of the instrument in configs. A-D. Only noise mitigation components in the external region were used, and components *h* and *i* were not installed for these experiments. Comparison among measurements in configs. A-D shows a precipitous decline in noise levels when the magnets and shielding were installed (config. C). Addition of an electrostatic bias (config. D) did not affect the noise level but did reduce the variability. This suggests that the excess noise level of config. A depicted in Fig. 3 was largely due to low energy particles (largely stopped by the magnets), while its variability was due to higher energy ions (which are stopped by biasing the electrostatic grating). The total noise was reduced by an order of magnitude between configs. A and D (approximately 43 μA).

Table II(b) shows the comparison of tests using secondary electron suppression features in the internal region of the instrument in configs. D-H [with config. D repeating from Table II(a)]. For all of these tests, components *d* and *e* were installed and *f* was held at a positive bias. Comparison among measurements in configs. D-H reveals similar efficacy of the electrostatic biasing (config. E) and efficacy of the magnets (config. F) at suppressing secondary electrons, suggesting that the excess noise in config. D is dominated by UV-induced photoemission from detector elements. Combining biasing with magnets (config. G) grants a larger reduction in the noise level. The addition of internal insulating shields *i* initially resulted in a larger positive noise level in comparison to config. G. We interpret this as a reduction of secondary electrons from the bias grating *g* impacting the detector grating *b*. Adjusting the internal bias to -40 V reduces secondary electrons from the detector elements, which balances the noise level nearer to zero (yet does not eliminate it). The total noise between configs. D and H was reduced by more than two orders of magnitude.

The application of all magnetic and electrostatic noise mitigation features has reduced the noise measured by the prototype detector by over 3 orders of magnitude, from 47 μA in config. A to approximately 20 nA in config. H. This remaining noise is likely dominated by photoelectric loss from the edges of the detector elements and any stray ions entering the instrument with energies over 500 eV.

V. CONCLUSIONS

We have implemented a series of hardware features that use electric and magnetic fields along with physical shielding

to provide particle and radiation mitigation and secondary electron suppression. These features have enabled operation of the detector with a direct view of a high temperature plasma. Measurements made during improved confinement periods of MST plasmas have shown that the features can reduce noise levels and variability from tens of microamps to tens of nanoamps. The instrument features implemented to reduce noise have also helped identifying the source of the noise, which is dominated by plasma ions and UV radiation.

SUPPLEMENTARY MATERIAL

See [supplementary material](#) for the data shown in Fig. 3 in digital format.

ACKNOWLEDGMENTS

This material is based on the work supported by the U.S. Department of Energy, Office of Fusion Energy Sciences under Award No. DE-SC0006077.

This report was prepared as an account of work sponsored by an agency of the United States Government. Neither the United States Government nor any agency thereof, nor any of their employees, makes any warranty, express or implied, or assumes any legal liability or responsibility for the accuracy, completeness, or usefulness of any information, apparatus, product, or process disclosed, or represents that its use would not infringe privately owned rights. Reference herein to any specific commercial product, process, or service by trade name, trademark, manufacturer, or otherwise does not necessarily constitute or imply its endorsement, recommendation, or favoring by the United States Government or any agency thereof. The views and opinions of authors expressed herein do not necessarily state or reflect those of the United States Government or any agency thereof.

- ¹P. J. Fimognari, T. P. Crowley, and D. R. Demers, *Rev. Sci. Instrum.* **87**, 11D414 (2016).
- ²T. P. Crowley, D. R. Demers, and P. J. Fimognari, *Rev. Sci. Instrum.* **87**, 11D418 (2016).
- ³G. Tonetti and K. A. Connor, *Plasma Phys.* **22**, 361 (1980).
- ⁴T. P. Crowley, *Rev. Sci. Instrum.* **59**(8), 1638 (1988).
- ⁵D. R. Demers, K. A. Connor, J. Lei, P. M. Schoch, and U. Shah, *Rev. Sci. Instrum.* **72**(1), 568 (2001).
- ⁶P. J. Fimognari, D. R. Demers, X. Chen, and P. M. Schoch, *Rev. Sci. Instrum.* **85**(11), 11D849 (2014).
- ⁷J. A. Beckstead, S. C. Aceto, T. P. Crowley, D. R. Demers, P. E. McLaren, A. Ouroua, J. G. Schatz, and P. M. Schoch, *Rev. Sci. Instrum.* **68**(1), 328 (1997).
- ⁸I. S. Nedzelskiy, N. B. Dreval, S. M. Khrebtov, A. D. Komarov, A. S. Kozachok, and L. I. Krupnki, *Rev. Sci. Instrum.* **72**(1), 575 (2001).
- ⁹R. B. Henriques, I. S. Nedzelskiy, A. Malaquias, and H. Fernandes, *Rev. Sci. Instrum.* **83**, 10D705 (2012).
- ¹⁰R. N. Dexter, D. W. Kerst, T. W. Lovell, S. C. Prager, and J. C. Sprott, *Fusion Technol.* **19**, 131 (1991).
- ¹¹N. Lanier, Ph.D. thesis, University of Wisconsin Madison, 1999.
- ¹²D. R. Demers and P. J. Fimognari, *Rev. Sci. Instrum.* **83**, 10D711 (2012).